Manipulating Light with a Magnetic Field

Bart A. van Tiggelen[1] and Geert L. J. A. Rikken[2]

[1] CNRS/Laboratoire de Physique et Modélisation des Milieux Condensés
Université Joseph Fourier, Maison des Magistères,
B.P. 166, 38042 Grenoble, France
`tiggelen@belledonne.polycnrs-gre.fr`
[2] Grenoble High Magnetic Field Laboratory, Max Planck Institut für
Festkörperforschung/CNRS, B.P. 166, 38042 Grenoble, France

Abstract. We review our theoretical and experimental work done on light propagation and scattering in magnetic fields.

1 Introduction

For more than one century, we have known that Maxwell's equations provide a complete description of the propagation of classical electromagnetic waves. For applications in daily life, it has become customary to describe the interaction of matter on a macroscopic level, i. e., without worrying about individual atoms, but looking only at charge distributions on scales large compared to the atomic scale. Microscopic charges and currents are described by the polarization density vector $\boldsymbol{P}$ and the magnetization $\boldsymbol{M}$. It is important to realize that this description is only approximate. Cases are known for which the macroscopic Maxwell equations seem to break down since they do not predict the observed behavior [1,2,3]. Macroscopically, it is still possible to consider a charge density ρ and a current density $\boldsymbol{J}$, but we will focus on dielectric materials for which both of them vanish.

A solution of Maxwell's equations becomes feasible when so-called *constitutive* relations are put forward that relate the microscopic parameters $\boldsymbol{P}$ and $\boldsymbol{M}$ to the macroscopic electromagnetic fields $\boldsymbol{E}$ and $\boldsymbol{B}$. Constitutive relations are subject to symmetry relations [4]. For instance $\boldsymbol{P}$ is, like the electrical field $\boldsymbol{E}$, a polar (parity-odd) vector that changes sign upon space inversion. On the other hand, the magnetic field $\boldsymbol{B}$ is a pseudovector, invariant under a space inversion, but variant upon time-reversal. One symmetry allowed, a constitutive relation for the polarization density $\boldsymbol{P}$ could be [4]

$$\boldsymbol{P} = \chi_0 \boldsymbol{E} + \chi_1 \partial_t \boldsymbol{E} \times \boldsymbol{B} + \chi_2 (\boldsymbol{B} \cdot \boldsymbol{B}) \boldsymbol{E} + \chi_3 (\boldsymbol{E} \cdot \boldsymbol{B}) \boldsymbol{B} + \cdots . \qquad (1)$$

For simplicity, we have adopted an isotropic medium so that all constitutive parameters χ_n are scalars and not second-rank tensors. In the above equation, many other terms are possible, and we have — for future use — just collected the terms linear in the electrical field and without time derivatives of the magnetic field. They are still nonlinear in the magnetic field, which complicates

the solution of the macroscopic Maxwell equations. A dramatic simplification occurs if the magnetic field $\boldsymbol{B}$ is in fact a low-frequency, external field $\boldsymbol{B}_0$ that is orders of magnitude larger than that of the electromagnetic field itself. In that case, the constitutive relation linearizes to

$$\boldsymbol{P}(\omega) = \boldsymbol{\chi}(\omega, \boldsymbol{B}_0) \cdot \boldsymbol{E}(\omega) \,, \tag{2}$$

with the electrical susceptibility tensor,

$$\chi_{ij}(\omega, \boldsymbol{B}) = \chi_0 \delta_{ij} + \chi_1 \omega \, i\epsilon_{ijk} B_k + \chi_2 B^2 \delta_{ij} + \chi_3 B_i B_j \,. \tag{3}$$

We have inserted harmonic waves with frequency ω. The dielectric tensor is defined as $\boldsymbol{\varepsilon} \equiv 1 + \boldsymbol{\chi}$. The constitutive relation above is purely linear in the electromagnetic field $\boldsymbol{E}$ and demonstrates that magneto-optics can be considered a particular case of nonlinear optics. If we disregard the existence of the microscopic magnetization $\boldsymbol{M}$, an "unwarrantable refinement at optical frequencies" according to *Landau*, *Lifshitz* and *Pitaevskii* [5], Maxwell's equations and the constitutive equation (2) for $\boldsymbol{P}$ can be combined to give one linear "Helmholtz equation",

$$\boldsymbol{\nabla} \times \boldsymbol{\nabla} \times \boldsymbol{E}(\omega, \boldsymbol{r}) + \frac{\omega^2}{c_0^2} \boldsymbol{\chi}(\boldsymbol{r}, \boldsymbol{B}_0) \cdot \boldsymbol{E}(\omega, \boldsymbol{r}) = \frac{\omega^2}{c_0^2} \boldsymbol{E}(\omega, \boldsymbol{r}) \,. \tag{4}$$

The fascinating analogy of this equation to the Schrödinger eigenvalue equation has frequently been emphasized [6,7,8] and is often of great use in finding its solutions, using results from quantum mechanics. As in Schrödinger's theory, conservation of electromagnetic energy is guaranteed when the electromagnetic "potential" $\boldsymbol{\chi}$ is a hermitan operator, i. e., $\chi_{ij} = \bar{\chi}_{ji}$. This happens when all coefficients χ_n in (3) are real-valued.

2   Magneto-Optics of Homogeneous Media

Local, homogeneous media are characterized by a susceptibility that is independent of $\boldsymbol{r}$. Equation (4) can now easily be solved upon inserting plane waves,

$$\boldsymbol{E}(\omega, \boldsymbol{r}) = \boldsymbol{e}(\omega, \boldsymbol{k}) \exp(\mathrm{i}\boldsymbol{k} \cdot \boldsymbol{r}) \,, \tag{5}$$

with a yet unknown polarization vector $\boldsymbol{e}$. The wave equation (4) reduces to the so-called "Fresnel equation",

$$\det \left[\boldsymbol{k}^2 - \boldsymbol{k}\boldsymbol{k} - \frac{\omega^2}{c_0^2} - \boldsymbol{\chi}(\boldsymbol{B}_0)\omega^2 \right] = 0 \,, \tag{6}$$

which provides the complex dispersion law $\omega(\boldsymbol{k})$.

The different terms in (3) correspond to different well-known magneto-optical effects. Let us first concentrate on the term χ_2 in (3). We easily obtain the dispersion law given by

$$n^2 \frac{\omega^2}{c_0^2} \approx \left(\boldsymbol{k} \pm \frac{V c_0}{n} \boldsymbol{B}_0 \right)^2 , \tag{7}$$

where we dropped small terms quadratic in the magnetic field and introduced the complex index of refraction $n \equiv \sqrt{1 + \chi_0}$, as well as the Verdet constant $V \equiv \frac{1}{2}\chi_1\omega^2$. If χ_0 and χ_1 are both real-valued, (7) locates the "constant-frequency" surfaces in $\boldsymbol{k}$ space around two spheres, translated over a distance VB/n from the origin along and opposite to the magnetic field (Fig. 1). Their separation is largest when the $\boldsymbol{k}$ vector is parallel to the magnetic field (the so-called "Faraday" geometry) and vanishes when they are mutually orthogonal (the "Voigt" geometry). The two spheres lift the degeneracy of the two states of circular polarization $\pm$, resulting in two different group velocities for different circular polarizations. For linearly polarized light in the Faraday geometry, this leads to a rotation of the polarization vector along the magnetic field over an angle VBr, with r the distance of propagation. This is called the Faraday effect. If χ_0 has an imaginary part, the light will be absorbed. A nonzero value of $\mathrm{Im}\,\chi_1$ implies different absorption for different states of circular polarization. This is called magnetic circular dichroism (MCD).

The terms involving χ_2 and χ_3 in (3) are quadratic in the magnetic field and generate a uniaxial symmetry in the dielectric tensor. The resulting linear birefringence is called the Cotton–Mouton effect. This effect is often much smaller than the Faraday effect and has a crucial difference from the Faraday effect. Only the Faraday effect satisfies the relations,

$$\varepsilon_{ij}(\boldsymbol{B}_0) = \varepsilon_{ji}(-\boldsymbol{B}_0) \neq \varepsilon_{ji}(\boldsymbol{B}_0) . \tag{8}$$

The equality is a general consequence of the time-reversal symmetry of matter + magnet [5]; the minus-sign is due to the fact that the magnetic field is
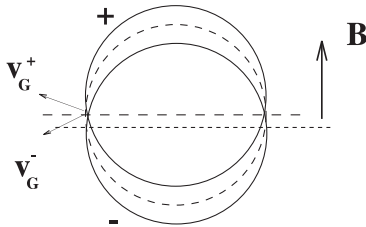

Fig. 1. Dispersion law for the Faraday effect. The degeneration of the two circular states $\pm$ of polarization is lifted. Their constant frequency surface is shifted along or opposite to the magnetic field. They remain degenerate only for wave vectors perpendicular to the magnetic field, but the group velocity for both modes is deflected along the magnetic field

a pseudovector. The inequality implies that the Faraday effect, contrary to the Cotton–Mouton effect, breaks time-reversal symmetry only in the subsystem of matter. This aspect gives the Faraday effect an important role in the more general context of light propagation in the presence of broken symmetries.

2.1 Magnetodeflection of Light

The bending of electrons in a magnetic field caused by the Lorentz force lies at the very base of many electronic phenomena in disordered metals and semiconductors, such as the Hall effect and the magnetic suppression of weak localization. The question naturally arises whether light propagating in non-scattering, homogeneous media is also deflected by a static transverse magnetic field. Some aspects of the deflection of light by a magnetic field have already been discussed in [5]. Those effects, as has been estimated, are very small [9], which may explain why, to our knowledge and surprise, they have never been observed until recently. A different kind of magnetodeflection has been reported in absorbing homogeneous media [10]. The question whether light is bent by magnets in homogeneous media has recently been raised again by *'t Hooft* and *Van der Mark* [11]. This topic is part of a much broader discussion on the properties of macroscopic electromagnetic fields inside dielectrics, that still yields new results, despite its long history [12,13].

In a nonabsorbing medium, the direction of wave propagation is unambiguously given by the group velocity $\boldsymbol{v}_\mathrm{G} = d\omega/d\boldsymbol{k}$. The absence of absorption also guarantees that $\boldsymbol{v}_\mathrm{G}$ is parallel to the Poynting vector $\boldsymbol{S} = (c_0/4\pi)\,\boldsymbol{E}\times\boldsymbol{B}$, a theorem that is left as an exercise in [5]. From (7), for the group velocity in the presence of the Faraday effect,

$$\boldsymbol{v}_\mathrm{G}^\pm = \frac{c_0}{n}\,\widehat{\boldsymbol{k}} \pm \frac{V c_0^2}{\omega n^2}\,\boldsymbol{B}_0\,. \tag{9}$$

On the basis of this equation, the optical energy flow can be deflected by a magnetic field. We note that the deflection is only in the direction of the magnetic field and no "magnetotransverse" term, perpendicular to both magnetic field and wave vector is present.

From Maxwell's equations, we can calculate the Poynting vector $(c_0/4\pi)$ $\boldsymbol{E}\times\boldsymbol{B}$,

$$\boldsymbol{S}_\pm(\boldsymbol{B}_0) \propto \operatorname{Re} n\widehat{\boldsymbol{k}} \pm \operatorname{Re}\left(\frac{V c_0 \overline{n}}{\omega n}\right)\boldsymbol{B}_0 + \operatorname{Im}\left(\frac{V c_0 \overline{n}}{\omega n}\right)\widehat{\boldsymbol{k}}\times\boldsymbol{B}_0\,. \tag{10}$$

In this expression, we have allowed for absorption and magnetic circular dichroism. They cause differences between the directions of the Poynting vector and the group velocity. In particular, the Poynting vector contains a magneto-transverse component $\widehat{\boldsymbol{k}}\times\boldsymbol{B}_0$.

In nonlocal media, the electromagnetic current density is known to be different from the Poynting vector [5,14,15]. In media with local response,

the Poynting vector is widely accepted as the current density. The conflict above with the group velocity puts the validity of the Poynting vector as the energy flow at stake in absorbing media. Arguments based on energy conservation and macroscopic Maxwell equations show that the energy flow of an electromagnetic wave is given by the more general expression

$$\widetilde{\boldsymbol{S}} \equiv \frac{c_0}{4\pi}\boldsymbol{E} \times \boldsymbol{B} + \nabla \times \boldsymbol{T}\,, \tag{11}$$

where $\boldsymbol{T}$ is some vector field to be determined [16]. The ambiguity in the energy flow, reflected by the existence of the second term in (11), is well appreciated in standard textbooks on electrodynamics [4,16,17,18] but is always discarded.

2.2   Bending of Light by Magnetic Fields

To experimentally test the various predictions for the direction of energy flow, we determined the deflection of light upon propagation in several homogeneous dielectrics in a transverse magnetic field [19]. The setup is shown schematically in Fig. 2. A light beam of a given polarization state is normally incident on the sample, placed in a transverse magnetic field, alternating at 8 Hz. The transmitted light is detected by two-quadrant split photodiodes, whose interconnecting axis can be directed along the $\boldsymbol{B}_0$ axis or the $\boldsymbol{k} \times \boldsymbol{B}_0$ axis. The difference between the photodiode signals represents a magnetic-field-induced lateral displacement of the beam after passage through the sample. From (10), it is clear that this displacement can be determined by subtracting the $\boldsymbol{B}_0$ axis displacement signals for left- and right-circularly polarized light, according to

$$\frac{\boldsymbol{S}_+(\boldsymbol{B}_0) - \boldsymbol{S}_-(\boldsymbol{B}_0)}{S} = \frac{2Vc_0}{n\omega}\boldsymbol{B}_0\,. \tag{12}$$
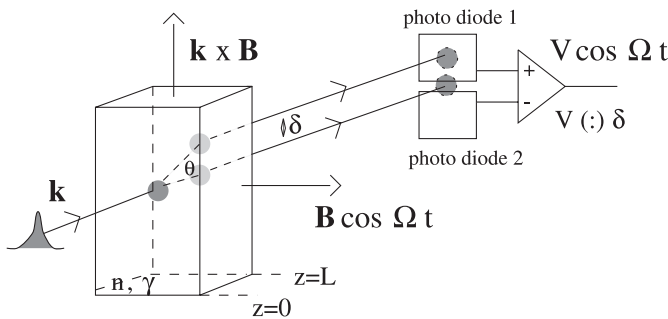

Fig. 2. Schematic setup of the deflection experiment. As shown, the displacement of the beam in the $\boldsymbol{k} \times \boldsymbol{B}$ direction is detected. By rotating the photodiode assembly over 90° along $\boldsymbol{k}$, the $\boldsymbol{B}$ axis displacement is detected. Taken from *Rikken* and *Van Tiggelen* [19]

Figure 3 confirms the displacement *along* the magnetic field, predicted by (9). Note that the observed deflection is only of the order of 10^{-7} radians. Our estimated inaccuracy is well below this value. This is the *first* experimental observation of deflection of light in a magnetic field. The good agreement with theory also gives us confidence in our experimental setup.

A comment on these conclusions was published by *'t Hooft, Nienhuis*, and *Paaschens* [20]. They argued that *exactly* in Voigt geometry, the eigenmodes are both linearly polarized, none of which suffer from magnetodeflection. They explained our experiments by a "misalignment" of only 10^{-7} mrad of the magnetic field. Their considerations are correct but do not affect the magnetodeflection predicted by (12) [21]. Our He–Ne laser has a nearly diffraction-limited angular divergence of 10^{-3} mrad. The photodiodes measure the deflection of the *intensity weighted* wave vector average. Therefore, only a fraction of 10^{-4} of the light flux propagates within the critical range. This fraction will not be deflected. The remainder behaves conform to our description using circularly polarized eigenmodes. For our experiment, the improved deflection theory of *'t Hooft* et al., therefore, would introduce a relative correction in the deduced deflection angle of the beam of 10^{-4}, which is far below the experimental relative uncertainty of this angle ($\pm 5 \times 10^{-2}$).

We have also carefully looked for the magnetotransverse bending present in the Poynting vector (10) and proportional to the magnetic circular dichroism $\mathrm{Im}\,V$. Experimentally, we found no significant deflection at the level of two orders of magnitude below the theoretical prediction of (10) [19]. To our
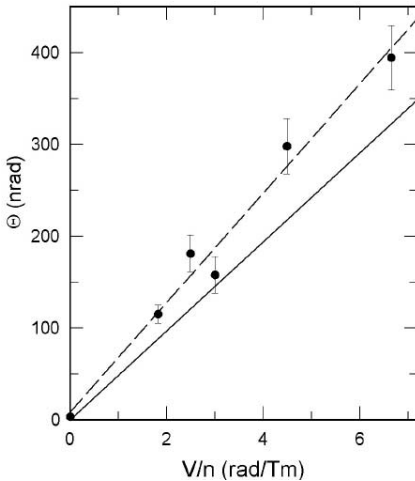

Fig. 3. $\widehat{B}$ axis displacement δ versus sample length L [laser wavelength 632.8 nm, sample material is Plexiglas ($n = 1.49$, $V = 4.5$ mrad/Tm) and magnetic field strength $B = 0.48$T.] *Dashed line* is a linear fit to the data points. *Inset* shows the dependence of the deflection angle $\theta = \delta/L$ on magnetic field strength, also for Plexiglas. *Dashed line* is a linear fit to the data points

knowledge, this is the first time that the widely accepted Poynting vector definition, its direction in particular, is experimentally proven to be incorrect and that the more general relation (11) must be invoked. The absence of a magnetotransverse deflection in homogeneous absorbing media emphasizes the different impact of a magnetic field on absorbing and scattering media; as will be shown below, the latter exhibits such a reflection.

It seems indeed possible to find a choice for T that reconciles the energy flow as expressed by (11) with the group velocity, which in turn is consistent with our experimental observation. We emphasize that this choice is not necessarily unique. Although we have not clarified the physical significance of such remarkable, albeit unavoidable, choices for T, these findings contribute to the ongoing discussion on the interpretation of the Poynting vector as the flow of electromagnetic energy [23].

3 Magneto-Optics of Heterogeneous Media

3.1 Single Magneto-Mie Scattering

To undertake a study of magneto-optics of heterogeneous media, one is obliged first to understand the magneto-optics of one small spherical particle. Already in the 1970s, *Ford* and *Werner* [24] made an extensive study of magneto-Mie scattering. The small perturbation of the Faraday effect, of the order of 10^{-4}, to the standard Mie problem [25], justifies a perturbation theory linear in the magnetic field, quite similar to the standard treatment of the Zeeman effect in atomic orbitals.

The first-order magneto-optical change in the differential cross section $\mathrm{d}\sigma/\mathrm{d}\Omega(\boldsymbol{k} \rightarrow \boldsymbol{k}')$ can be guessed from symmetry arguments. Let us consider a Mie sphere made of a dielectric constant given by (3). Being a scalar, the magneto cross section linear in $\boldsymbol{B}_0$ must be proportional to either $\boldsymbol{k} \cdot \boldsymbol{B}_0$, $\boldsymbol{k}' \cdot \boldsymbol{B}_0$ or $\det(\boldsymbol{k}, \boldsymbol{k}', \boldsymbol{B}_0)$. Being pseudoscalars, the first two options are parity-forbidden. The *only* expression allowed by symmetry and linear in the magnetic field is

$$\frac{1}{\sigma_{\mathrm{tot}}} \frac{\mathrm{d}\sigma}{\mathrm{d}\Omega}(\boldsymbol{k} \rightarrow \boldsymbol{k}'; \boldsymbol{B}_0) = F_0(\theta) + F_1(\theta) \det(\boldsymbol{k}, \boldsymbol{k}', \boldsymbol{B}_0). \tag{13}$$

This cross section also obeys the reciprocity principle

$$\frac{\mathrm{d}\sigma}{\mathrm{d}\Omega}(\boldsymbol{k} \rightarrow \boldsymbol{k}'; \boldsymbol{B}_0) = \frac{\mathrm{d}\sigma}{\mathrm{d}\Omega}(-\boldsymbol{k}' \rightarrow -\boldsymbol{k}; -\boldsymbol{B}_0). \tag{14}$$

$F_0(\theta)$ is the phase function of the conventional Mie problem [25] and — by rotational symmetry — depends only on the angle θ between $\boldsymbol{k}$ and $\boldsymbol{k}'$. For the same reason, F_1 can depend only on the angle θ. In [26], we developed a method for calculating $F_1(\theta)$. For a Rayleigh scatterer, the Born approximation can be used which leads to $F_1(\theta) \sim (V/k) \cos\theta$.

It is well known that for applications in multiple scattering, the anisotropy of the cross section is important [6]. For Mie spheres, this anisotropy is quantified by the "anisotropic factor" $\langle \cos\theta \rangle$, which is $\cos\theta$ averaged over $F_0(\theta)$. This factor discriminates forward ($\cos\theta > 0$) from backward ($\cos\theta < 0$) scattering. In magneto-Mie scattering, a second anisotropy shows up that discriminates "upward" from "downward" scattering (Fig. 4). If the magnetic field is perpendicular to both the incident and outgoing wave vectors, (13) predicts a difference between upward and downward flux, both defined with respect to the magnetotransverse direction $\boldsymbol{k} \times \boldsymbol{B}_0$. The magnetoanisotropy η_1 of one scatterer can be quantified exactly as the normalized difference between total flux upward and total flux downward. An easy calculation yields [26]

$$\eta_1 \equiv 2\pi \int_0^\pi \mathrm{d}\theta \sin^3\theta F_1(\theta). \tag{15}$$

If $\eta_1 \neq 0$, we shall speak of "magnetotransverse light scattering." No magnetotransverse anisotropy survives for one Rayleigh scatterer, as can easily be checked by filling in $F_1 \sim \cos\theta$. At least two Rayleigh scatterers are required to generate a net effect [26], or, alternatively, a Mie sphere with finite size (Fig. 5).
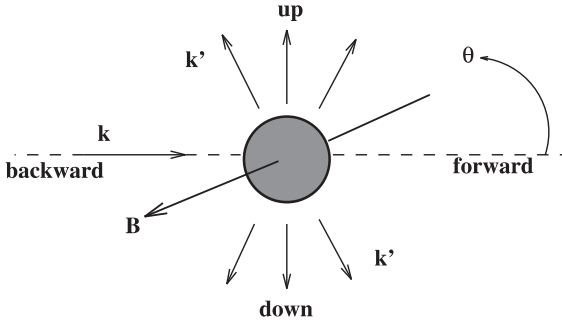

Fig. 4. Scattering geometry for magnetotransverse scattering from a Mie sphere, given an incident plane wave from the left

3.2   Multiple Magnetoscattering of Light

In principle, when the medium is heterogeneous, light is scattered and concepts like "Faraday rotation" become ill-defined. Even in a random medium, it seems possible to define a dielectric constant associated with the "effective medium". When small particles of the heterogeneous medium are magnetoactive, the effective medium is undoubtedly magnetoactive as well. The wave will undergo a Faraday effect on its way from one scatterer to the other. Since
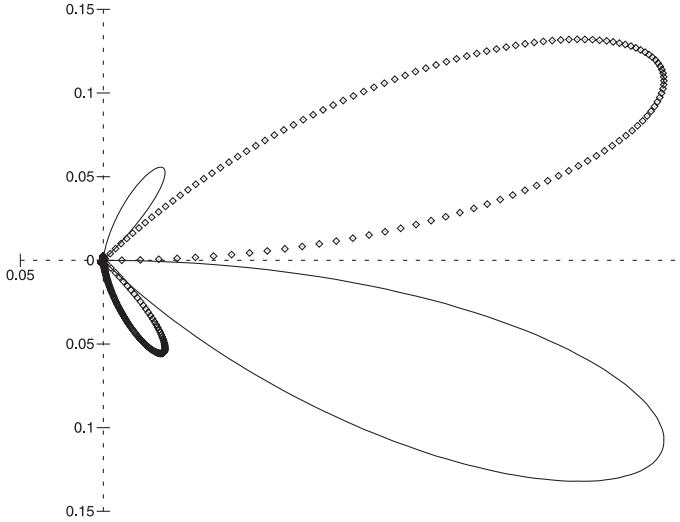
Fig. 5. Polar plot of the phase function associated with the magneto cross section of Mie scatterers with size parameter $x = 2\pi a/\lambda = 5$. *Solid line* denotes positive magneto cross section, *symbols* denote negative magneto cross section. Magnetic field is directed perpendicular to the plot. Taken from *Lacoste* et al. [26]

the typical distance between two scattering events is typically the mean free path ℓ, we expect a typical Faraday rotational angle of

$$\alpha \approx V_{\text{eff}} B\ell \cos\theta \,, \tag{16}$$

with V_{eff} some effective medium Verdet constant and θ the angle between the wave vector and the magnetic field. If the matrix is inert and the scatterers have a Verdet constant V and volume fraction f, the choice $V_{\text{eff}} \approx fV$ does not *a priori* seem unreasonable.

Alternatively, the Faraday effect can be understood as a magnetically induced phase shift $\phi = \sigma V_{\text{eff}} B\ell \cos\theta$ of a wave with circular polarization σ. Since multiple scattering tends to randomize the state of circular polarization, the magnetic field induces a net zero phase shift of a wave. This excludes the Faraday effect as a direct phenomenon in multiple scattering. Nevertheless, novel effects in multiple scattering can exist that have the Faraday effect at their origin. The typical fluctuation of the magnetically induced phase shift in multiple scattering, $\sqrt{\langle\phi^2\rangle} \approx |V_{\text{eff}} B\ell|$, is likely to be a parameter quantifying the impact of Faraday effect in multiple scattering, just like the parameter $\omega_c\tau$ (the cyclotron motion executed by an electron during one mean free time) is known to quantify magnetic effects in electronic transport. Three magneto-optical scattering phenomena are now known to exist: the photonic Hall effect, photonic magnetoresistance, and the magnetic supression of coherent backscattering.

The influence of a magnetic field on coherent backscattering will not be discussed here. Experimental work by *Maret* et al. demonstrated that interference phenomena in multiple scattering are suppressed by an external magnetic field due to the broken time-reversal symmetry [27]. The universal parameter governing the suppression is indeed found to be $V_{\text{eff}}B_0\ell$ [28], as confirmed by numerical simulations [29] and calculations with point scatterers [30] as well as Mie spheres [31].

The physics of multiple scattering can best be understood by adopting a diffusion picture for the multiply scattered light. This familiar picture asserts that the average local current density $\boldsymbol{J}$ is due to a gradient in electromagnetic energy density $\boldsymbol{\nabla}\rho$. The so-called Fick's law reads [6],

$$\boldsymbol{J}(\boldsymbol{r}) = -\boldsymbol{D} \cdot \boldsymbol{\nabla}\rho(\boldsymbol{r}), \tag{17}$$

with D_{ij} the diffusion tensor. Because the current and the gradient are both parity-odd vectors, $\boldsymbol{D}$ must be parity-even. Fick's law breaks time-reversal symmetry since $\boldsymbol{D}$ is believed to be a positive definite tensor, and only the current changes sign upon time-reversal. This symmetry breaking is due to the ensemble-average that has been assumed implicitly in (17) and makes macroscopic transport phenomena irreversible.

The impact of a magnetic field on light diffusion can be understood qualitatively by realizing that the magnetic field is a pseudovector. Onsager relations apply to transport coefficients and thus also to the diffusion tensor,

$$D_{ij}(\boldsymbol{B}_0) = D_{ji}(-\boldsymbol{B}_0), \tag{18}$$

so that,

$$\begin{aligned}D_{ij}(\boldsymbol{B}_0) = D_0\delta_{ij} &+ D_{\text{H}}(B_0)\epsilon_{ijk}(B_0)_k \\ &+ D_\perp\left(\delta_{ij}B_0^2 - (B_0)_i(B_0)_j\right) + D_\parallel(B_0)_i(B_0)_j.\end{aligned} \tag{19}$$

The first term is just the ordinary, isotropic diffusion tensor. The second term induces an energy current perpendicular to the energy gradient and the magnetic field, i.e., is magnetotransverse. In analogy to a similar effect for electrons in disordered semiconductors, we will refer to this as the *photonic Hall Effect* (PHE). The last two terms are quadratic in the magnetic field and make the current along the magnetic field different from that perpendicular. We will call this *photonic magnetoresistance* (PMR). Similar effects occur in the so-called Beenakker–Senftleben effect, describing the influence of a magnetic field on the thermal conductivity of paramagnetic and diamagnetic gases [32]. In the following subsections, we discuss the relation of these macroscopic effects to their microscopic equivalents discussed earlier, and report on their experimental verification.

3.3   Theory of Magnetodiffusion

One of the aims of multiple scattering theory is to establish a link between the macroscopic and the microscopic world. More specifically, we want to understand, qualitatively and quantitatively, the diffusion tensor (19) from the magneto cross section of one particle.

A rigorous theory for the photonic Hall effect was recently developed by *Lacoste* and *Van Tiggelen* [33,34]. Using a microscopic transport theory, a relation was found between the photonic Hall effect of one Mie particle, quantified by the parameter η_1 in (15), and the magnetotransverse diffusion D_H defined in (19),

$$\frac{D_H B_0}{D_0} = \frac{1}{2} \frac{\eta_1}{1 - \langle \cos \theta \rangle} = \frac{\pi}{1 - \langle \cos \theta \rangle} \int_0^\pi d\theta \sin^3 \theta F_1(\theta) . \tag{20}$$

Such a relation is intuitively reasonable, provided that single scattering is the basic building block of multiple scattering, which is true when the mean free path is much bigger than the wavelength. This was assumed in deriving (20). Perhaps less intuitive is the presence of the average cosine $\langle \cos \theta \rangle$ of the scattering cross section in (20). This parameter can be very close to one, as for large dielectric spheres [25], which greatly amplifies the relative importance of the photonic Hall effect. This factor was absent in an earlier calculation, which used Rayleigh point scatterers [35] but turned out to be important to come to a quantitative agreement between theory and experiments. Note that, by (20), D_H/D_0 should be independent of the scatterer concentration, provided it is small enough to ignore cluster effects.

In view of the familiar relation $D = \frac{1}{3} v_E \ell^*$ of the diffusion constant in terms of the speed of light and the mean free path ℓ^* [6], one can write the ratio $D_H B_0/D_0$ as a ratio of two transport mean free paths. This is more convenient for later purposes. This ratio can be used to define what we call the "photonic Hall angle". In electronic transport, this would be σ_{xy}/σ_{xx} with σ_{ij} the conductivity tensor, directly proportional to the diffusion tensor [36].

In Fig. 6, we show $\ell_\perp^*/\ell^*$ as a function of the size parameter, for a contrast in the index of refraction of $m \equiv n_S/n_m = 1.128$, corresponding to CeF_3 in glycerol. For particles sizes around 4 μm, we calculate $\ell_\perp^*/\ell^* = +0.06 V B \lambda$ which, for $V = -1100$ rad/Tm (at temperature T = 77 K) and vacuum wavelength $\lambda_0 = 0.457$ μm yields $\ell_\perp^*/\ell^* = -2 \times 10^{-5}$/T. The experimental value is $\ell_\perp/\ell^* \approx -1.1 \pm 0.3 \times 10^{-5}$/T for a 10 vol. % suspension [22].

A theory for the photonic magnetoresistance, i.e., the diffusion coefficients $D_\perp$ and $D_\parallel$ in (19), has so far been developed only for pointlike scatterers with Verdet constant V and volume fraction f [37], for which the prediction is

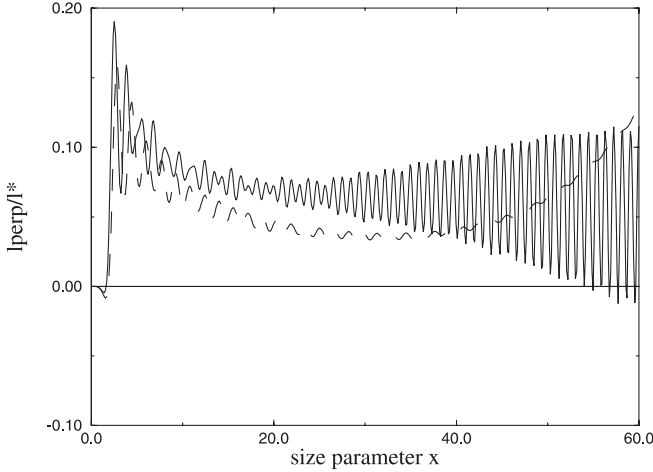$$\frac{D_\perp}{D_0} = -\frac{12}{5} (f V B_0 \ell)^2$$

Fig. 6. Ratio D_H/D_0 (photonic Hall angle) of magnetotransverse diffusion to isotropic diffusion, in units of the dimensionless parameter $2\pi V B/k$, as a function of size parameter $x = ka$ (a is the particle radius). *Solid line* corresponds to Mie spheres with index of refraction $m = 1.28$; *dashed line* is the Rayleigh–Gans approximation, valid as $m \to 1$. Taken from *Lacoste* and *Van Tiggelen* [33]

and

$$\frac{D_\parallel}{D_0} = -\frac{6}{5}\left(fVB_0\ell\right)^2 . \tag{21}$$

This calculation always implies a negative magnetoconductance (positive magnetoresistance) proportional to the typical fluctuations in the magnetically induced phase shift between two collisions. This property is expected to be valid in general. In the dilute regime, the ratios $D_{\perp,\parallel}/D_0$ are expected to be *independent* of the concentration of the scatterers.

3.4   Experiments on Magnetodiffusion

For experimental observation of the photonic Hall effect, scatterers with a large Verdet constant are required. This can be found in materials containing large concentrations of rare-earth ions like Ce^{3+}, Ho^{3+}, or Dy^{3+}. In these paramagnetic materials, the Verdet constant is inversely proportional to temperature and can thus be further enhanced by cooling.

The photonic magnetotransport phenomena were measured by phase-sensitive detection of the magnetically induced changes in the scattered and transmitted intensities. An alternating magnetic field $B_0(t) = B_0 \cos \Omega t$ with $B_0 \approx 1T$ and $\Omega \approx 40\,Hz$ was applied perpendicularly to the illuminating and collecting light guides. Monochromatic illumination was provided by an argon ion laser or with an incandescent lamp in combination with

a narrow-band interference filter. The scattered light was measured with silicon photo-diodes or photomultipliers outside the magnetic field region (see Fig.7). Both linear and quadratic magnetic field responses can be measured this way at the fundamental and second-harmonic frequencies Ω and 2Ω, respectively. The mean free path ℓ^* of the light in these scattering media was determined by measuring their optical transmission T by an integrating sphere and using $T = 1.6\,\ell^*/L$, where L is the sample thickness [38].

To deduce the various diffusion coefficients from our measurements, we have to know their relation to the current emerging from our cylindrical sample. This engineering part of the experiment was examined by solving the diffusion equation, with diffusion constant D_0 for a cylinder geometry with radius R and length L, with radiative boundary conditions at the surface and on the sides [38]. We adopted a source at a depth $x_0 \approx \ell$ at one side of the cylinder with a radial profile $J_{\rm in}(R)$ across the output of the multimode fiber used in the experiment. The magnetotransverse current can be calculated from this solution using Fick's law (17). These calculations demonstrated the following relation for the normalized photonic Hall effect:

$$\eta \equiv \frac{I_{\rm up} - I_{\rm down}}{\frac{1}{2}(I_{\rm up} + I_{\rm down})} = F\left(\frac{L}{R}\right)\frac{\ell_{\rm H}}{R}. \tag{22}$$

The function F depends only on the ratio of the length and width of the cylinder, not on the mean free path. For the experimental value $L/R = 2.6$, we estimated $F \approx 5$. A measurement of η thus gives direct access to the magneto-transverse transport mean free path $\ell_{\rm H}$.
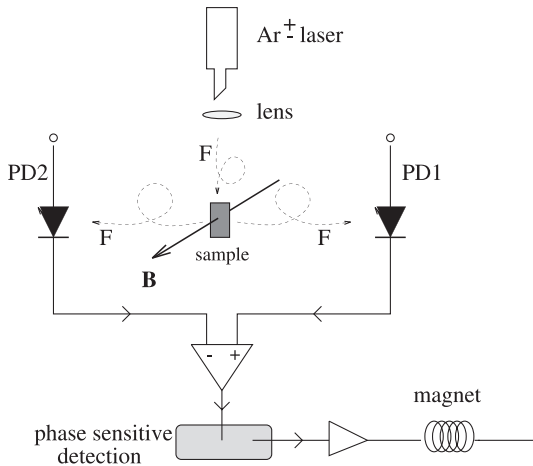

Fig. 7. Schematic setup for the observation of the photonic Hall effect. F = optical fiber, PD = photo-diode, $\boldsymbol{B}$ is the magnetic field

The role of sample geometry for the photonic magnetoresistance is easier to obtain since a slab geometry and an integrating sphere suffice. The total transmission coefficient, normalized to the one measured without magnetic field, is obtained from

$$\frac{\Delta T(\boldsymbol{B}_0 = \|, \perp)}{T} = \frac{D_{\|,\perp} B_0^2}{D_0} . \tag{23}$$

All geometry-dependent factors cancel since they are the same with and without the magnetic field.

3.4.1   Normal Photonic Hall Effect

The photonic Hall effect is qualified by the difference of transverse photon flux $\Delta I_\perp = I_L - I_R$, normalized by the transversely scattered intensity $I = \frac{1}{2}(I_L + I_R)$. This ratio should be proportional to the ratio of the magneto-transverse mean free path and the transverse dimension, as stated by (22). We estimate a systematic error of at least a factor of 2 in *attributing* values to ℓ_H and ℓ^* on the basis of Fick's law. Another uncertain factor is the broad size distribution of the scatterers.

The results shown in Fig. 8 confirm the predicted linear magnetic field dependences of this quantity. By normalizing it by the magnetic field, we obtain the photonic Hall effect per Tesla which is characteristic for a given scattering sample. Figure 9 shows the temperature dependence of the photonic Hall effect per tesla. As the only temperature-dependent parameter in the scattering process is the Verdet constant, the observed linear dependence on the
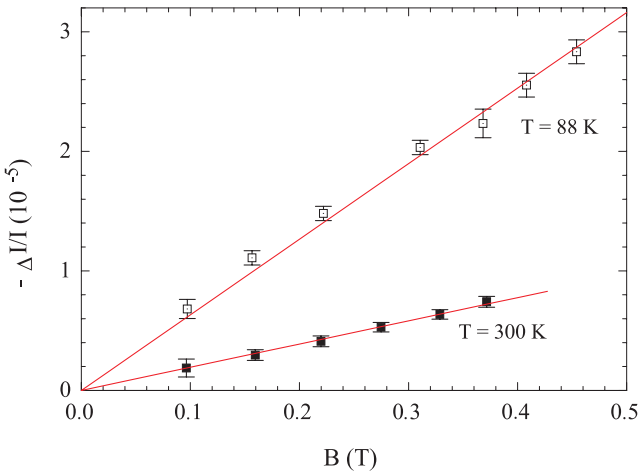

Fig. 8. Normal photonic Hall effect vs. magnetic field, showing linear behavior. Sample was EuF$_2$ in resin, observed with light of wavelength $\lambda = 457$ nm. Taken from *Rikken* et al. [42]
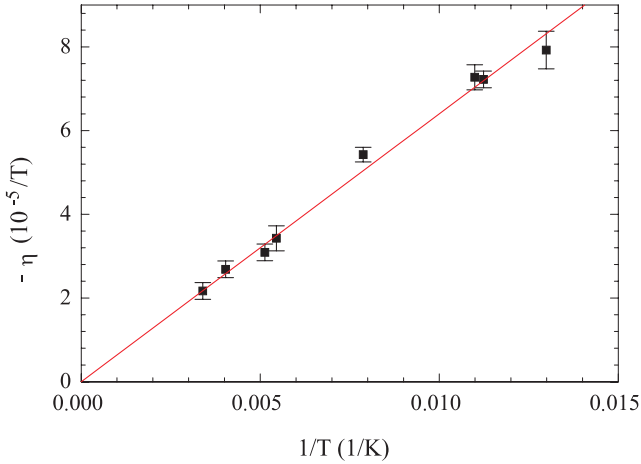
Fig. 9. Photonic Hall effect (per tesla) vs. temperature. The plot confirms the $1/T$ behavior predicted for paramagnetic scatterers. Sample was EuF_2 in resin, observed with light of wavelength $\lambda = 457\,\mathrm{nm}$. Taken from *Rikken* et al. [42]

inverse temperature confirms the linear relation between η and the Verdet constant. Figure 10 shows the mean free path ℓ^* and η as a function of the volume fraction of scatterers. We see that for large f, where ℓ^* becomes much smaller than the sample thickness and we are entering the multiple scattering regime, the Hall angle seems to become independent of f. The value for the magnetotransverse scattering length that we deduce at that point, using (22), is $\ell_H/B = -1\,\mathrm{nm/T}$, i.e., $\ell_H/\ell^* \approx -1.1 \times 10^{-5}/\mathrm{T}$, which is in good agreement with the Mie theory [33] discussed earlier. The inset shows the normalized photonic Hall effect for several different scatterers, as a function of the Verdet constant of the scatterers. The sign of the magnetotransverse photon flux was deduced from the phase angle of the lock-in. The linear relation that is observed, including the sign, cannot simply be explained by the linearity with the Verdet constant because the index of refraction also varies considerably among the different samples. Nevertheless, our magneto-Mie theory for CeF_3 theory reproduces this linearity for the photonic Hall effect assuming polydisperse samples containing ZnS, Al_2O_3, TiO_2, CeF_3, and EuF_2 [34]. The calculated photonic Hall effect changes rapidly as a function of particle size and can even change sign, but on average, the sign of the photonic Hall effect reflects the sign of the Verdet constant. The estimated anisotropic factor for our sample equals $\langle \cos\theta \rangle \approx 0.9$. Therefore, the amplification factor $1/(1 - \langle\cos\theta\rangle)$ for the photonic Hall effect is significant and improves theoretical predictions considerably for Rayleigh scatterers [35]. The pertinent role of the sign of the photonic Hall effect makes the analogy with the behavior of electrons and holes in the electronic Hall manifest again.
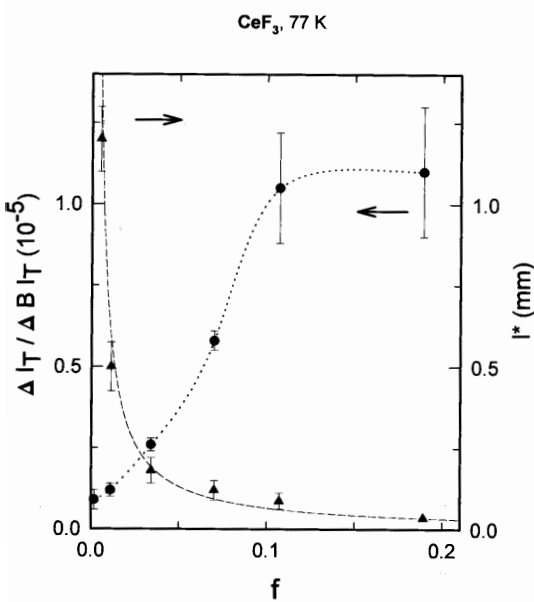
Fig. 10. Photonic Hall effect (per tesla) vs. volume fraction f of CeF$_3$ particles at a temperature $T = 77$ K. Also plotted is the transport mean free path as a function of volume fraction (*left vertical axis*) which decays basically as $1/f$ (*dashed*). Taken from *Rikken* and *Van Tiggelen* [21]

In this analogy, the Verdet constant of the scatterer takes over the role of electronic charge.

3.4.2   Photonic Hall Effect in Inverted Media

So far, we considered media with magnetoactive scatterers in a passive matrix. One might argue that in electronic magnetotransport, the effect of the magnetic fields occurs mainly between the scattering events. This raises the question whether a photonic Hall effect exists in "inverted" media, consisting of passive scatterers in a magnetoactive matrix.

The inverted medium is mathematically much more difficult to handle, and therefore no theoretical description is available at present. *Martinez* and *Maynard* [29] studied the inverted medium using a Monte-Carlo simulation but did not treat magnetodiffusion. Intuitively, there is no reason to believe that the photonic Hall effect differs from that in normal media. For volume fractions around $f \approx 50\%$, it is in fact impossible to discriminate between scatterers and matrix.

In the experiments [39], we used two different matrices, a saturated aqueous dysprosium chloride solution and a dysprosium nitrate glass. These are transparent apart from a few narrow and weak $4f$–$4f$ transitions of the

Dy^{3+} ion. The following values were found for the optical parameters at a wavelength of 457 nm: The refractive index of the solution $n_{\mathrm{m}} = 1.44$, the Verdet constant $V = -19\,\mathrm{rad/T\,m}$ at 300 K, the refractive index of the glass $n_{\mathrm{m}} = 1.53$, and its Verdet constant $V = -59\,\mathrm{rad/Tm}$ at 300 K. Scattering samples were prepared by adding Al_2O_3 particles to the matrix. The average size of these particles was 1 µm with a 50 % size dispersion. The refractive index of these scatterers was $n_{\mathrm{s}} = 1.72$. Their volume fraction f ranged between 0.5 and 10 %.

We measured ℓ^* as a function of the volume fraction f of the solution samples and found that over a large range of volume fractions, $\ell^* \propto f^{-1}$. Figure 11 confirms the predicted linear magnetic field dependence of the photonic Hall angle. It is important to note that the sign of the photonic Hall effect in inverted media with paramagnetic scatterers is the same as that obtained in normal media, where the magneto-optical activity is concentrated in paramagnetic scatterers. The temperature dependence is implied in Fig. 11. As the only temperature-dependent parameter in the scattering process is the Verdet constant, the observed linear dependence on the inverse temperature confirms the linear relation between the normalized photonic Hall effect and the Verdet constant of the matrix, which identifies the Faraday effect between the scatterers as its physical origin.
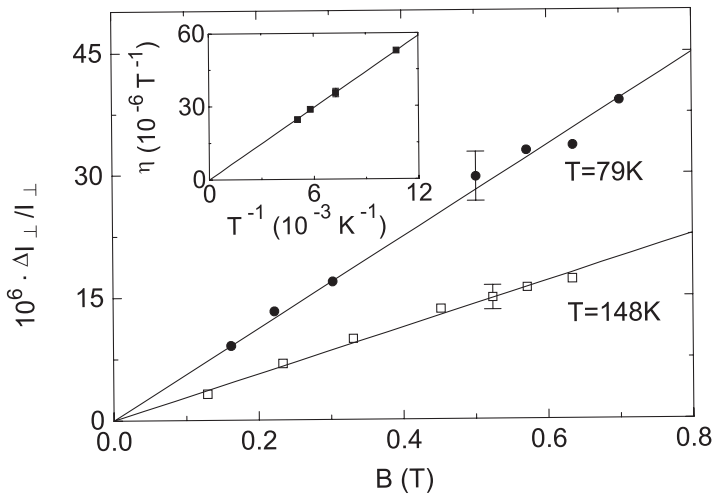

Fig. 11. Inverted photonic Hall effect vs. the magnetic field and the temperature (*inset*). As for the normal photonic Hall effect, the inverted photonic Hall effect is linear in the magnetic field and inversely proportional to temperature. Sample was Al_2O_3 particles with volume fraction $f = 4.2\,\%$ imbedded in a dysprosium nitrate glass. Wavelength of the light was $\lambda = 457\,\mathrm{nm}$. Taken from *Düchs* et al. [39]
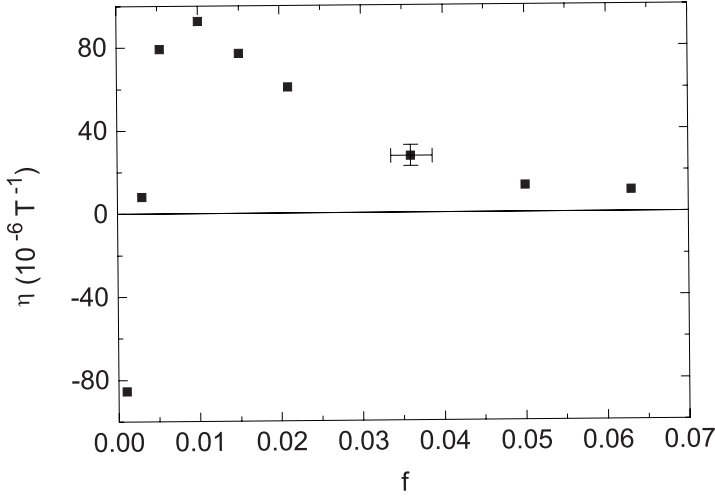
Fig. 12. Inverted photonic Hall effect vs. volume fraction of inert Al_2O_3 scatterers in a dysprosium nitrate glass, measured at a temperature $T = 77\,\mathrm{K}$. Taken from *Düchs* et al. [39]

The effect of scatterer concentration on the photonic Hall effect is shown in Fig. 12 for the glass samples. Upon decreasing the scatterer volume fraction, an increase in the normalized photonic Hall effect is obtained, until at a low volume fraction, the photonic Hall effect decreases and even changes sign. The increasing photonic Hall effect with decreasing volume fraction can be understood as a mean free path effect; Fig. 13 shows the photonic Hall effect as a function of the mean free path of the high volume fraction samples in the top panel of Fig. 12. It shows the linear dependence of the photonic Hall effect on the mean free path as long as this is much smaller than the sample dimensions, i. e., in the multiple scattering regime. For smaller volume fractions, i. e., longer mean free paths, this no longer holds and for the lowest volume fractions, one enters the single scattering regime which apparently gives an opposite sign for the magnetotransverse photon flux. The volume fraction at which this turnover occurs is higher for the glass samples because the refractive index difference between scatterer and matrix is smaller for these samples; so the mean free path is longer than for a solution sample at the same scatterer concentration.

For "normal" media, our experiments have shown empirically that the normalized photonic Hall effect in the multiple scattering regime is proportional to $V_{\mathrm{eff}} B \ell^*$ for the range of concentrations studied, where $V_{\mathrm{eff}} = f V_{\mathrm{s}}$ [22]. We now propose the empirical expression for arbitrary two-component media in the multiple scattering regime:

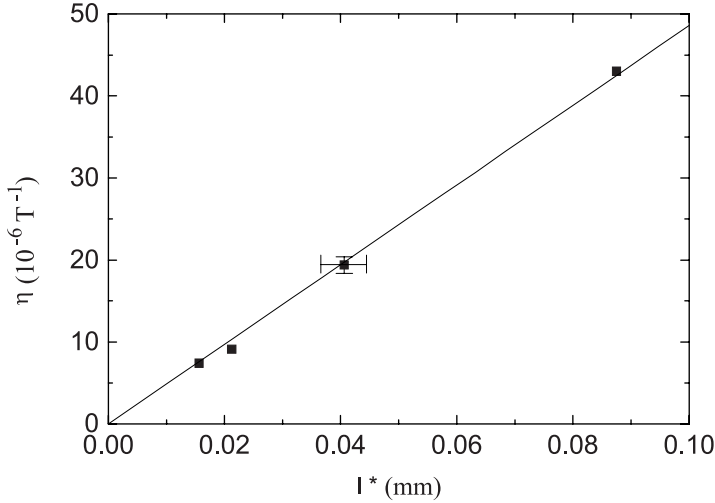$$\eta = G[fV_{\mathrm{s}} + (1-f)V_{\mathrm{m}}]\ell^* . \tag{24}$$

Fig. 13. Inverted photonic Hall effect vs. mean free path, measured in the multiple scattering regime (i. e., relatively large f in Fig. 12). Sample was the same as in Fig. 12. Taken from *Düchs* et al. [39]

The factor G can depend only on the shape of the sample, but this was not studied. For the experiments done so far, the value $G \approx 1 \times 10^{-2}$ covers both the normal and the inverted photonic Hall effect.

3.4.3 Photonic Hall Effect in Absorbing Media

Absorption is a specific property of classical waves and has no equivalent in charge transport. Therefore, we conducted experiments on the photonic Hall effect in the presence of absorption [40].

We first investigated the role of absorption in the scatterers. To that end, we used particles of HoF_3, obtained by chemical precipitation, and put them in a transparent, inert homogeneous matrix. The particles had an average radius $r \approx 0.5$ μm and a broad size distribution between $r = 0.2$ μm and $r = 5$ μm, that was determined using scanning electron microscopy. The Ho^{3+} ions have a narrow $4f$–$4f$ transition $^5I_8 \rightarrow^5 F_4$ around $\lambda \approx 534$ nm. By varying the wavelength of the diffusing light over a few tens of nanometers, we were able to scan across the absorption band, thereby strongly varying the imaginary part of the index of refraction κ_s, without significantly affecting the other optical parameters. The real part of the refractive index is $n_s = 1.6$ outside the absorption peak, and it varies only by 0.004 around the absorption peak.

The absorption spectrum in Fig. 14 was measured with a UV-vis spectrometer at room temperature from a thin slab of HoF_3 powder dispersed in an index-matched resin at 23 vol %. The absorption maximum blueshifts

from $\lambda = 534\,\text{nm}$ at $T = 300\,\text{K}$ toward $\lambda = 529\,\text{nm}$ at $T = 85\,\text{K}$. From the measurements carried out at $T = 300\,\text{K}$ on samples of different thickness, we concluded that the imaginary part of the refractive index is $\kappa_\text{s} \approx 0.0012$ at $\lambda = 535\,\text{nm}$ and $T = 300\,\text{K}$ and the absorption length in the multiple scattering samples is $L_\text{a} \approx 31 \pm 6\ \mu\text{m}$ at $\lambda = 535\,\text{nm}$. We assumed that these values stay the same at $T = 85\,\text{K}$ when corrected for the blueshift. Other optical parameters undergo only minor changes: the Verdet constant of HoF_3 is $\text{Re}\,V_\text{s} \approx 400\,\text{rad/Tm}$ and was seen to vary by only $20\,\%$ across the absorption band (Fig. 14a). The magnetic circular dichroism $\text{Im}\,V_\text{s}$ is estimated to be smaller than $1\,\text{rad/Tm}$ [41] in this spectral range. We estimate a variation $\Delta\,\ell^*/\ell^* \leq 0.25$ in the mean free path across the absorption band due to the change of the complex index of refraction $n_\text{s} + i\kappa_\text{s}$ with λ. The resin matrix had a refractive index $n_\text{m} \approx 1.566$ at $589\,\text{nm}$. Samples were prepared by mixing HoF_3 powder at a volume fraction of $f = 23\,\%$ with the liquid resin, followed by curing. We measured a transport mean free path $\ell^* \approx 70 \pm 26\ \mu\text{m}$ in the transparent spectral region of HoF_3.

We observed again a linear magnetic field dependence of $\Delta\,I_\perp/I_\perp$. This linear behavior was independent of the amount of absorption. Figure 15 contains the main result: It shows the normalized photonic Hall effect η as a function of wavelength around the absorption maximum. Outside the absorption band, we obtain negative values for η. These values agree in sign and magnitude with the results obtained in [22] and [42] for similar paramagnetic
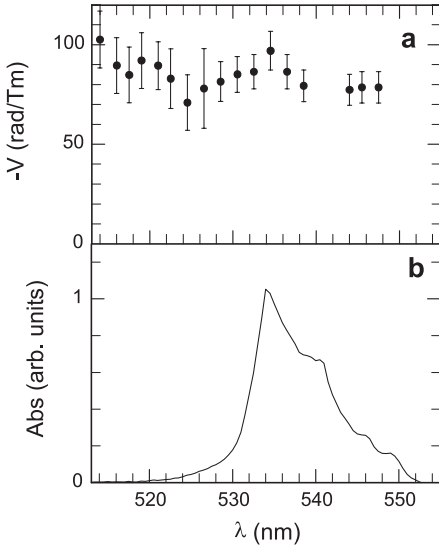

Fig. 14. Verdet constant (**a**) and absorption profile (**b**) for HoF_3 powder in resin, both at room temperature, around a wavelength of $535\,\text{nm}$. Taken from *Wiebel* et al. [40]
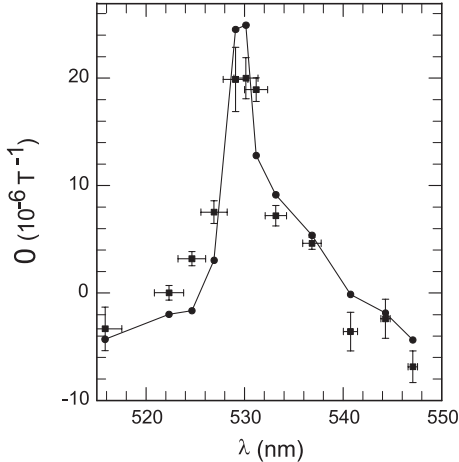
Fig. 15. Observed photonic Hall for a HoF_3 powder scanned along the absorption profile. The *solid line* is the prediction of Mie theory. Taken from *Wiebel* et al. [40]

scatterers. As the absorption increases, the photonic Hall effect η decreases to zero and rapidly changes sign around the absorption band center. The sign change of η seems to occur at the wavelength where L_a roughly equals ℓ^*. In the center of the absorption band, we obtain values for the photonic Hall effect that are roughly four times larger than those measured in the transparent region of HoF_3. At this wavelength, the absorption length $L_a \approx 31$ μm is smaller than ℓ^* and much smaller than the sample dimensions. As the maximum value of the photonic Hall effect coincides with the wavelength of maximum absorption, we conclude that the observed changes in the photonic Hall effect are dominated by absorption effects. Variations of other relevant optical parameters would have led to only minor changes in the photonic Hall effect.

To investigate the impact of absorption in the medium outside the scatterers, we prepared samples of similar, but transparent CeF_3 scatterers in the same resin matrix that was made absorbing by dissolving an organic dye into it. Values up to $\kappa_m \approx 0.001$ were obtained this way, i.e., comparable to the values of κ_s for the absorbing scatterers in the transparent matrix. We found *no significant variation* of the normalized photonic Hall effect η with increasing κ_m. Quite surprisingly, we see that the role of absorption in the matrix is very different from that of absorption in the magnetoactive scatterers.

The Mie theory developed by us to calculate the photonic Hall effect of spherical scatterers of arbitrary size [26,33] allows for the inclusion of absorption inside the scattering particles but does not allow for absorption in the matrix. In the calculation, we assume a complex refractive index $n_s + i\kappa_s(\lambda)$ and use $\kappa_s(\lambda)$ obtained from the absorption spectra in Fig. 14, corrected for the low temperature blueshift. We took $\mathrm{Re}\, V_s = 400$ rad/Tm and $\ell^* = 70$ μm

and completely disregarded $\operatorname{Im} V_s$. The geometry factor F in (22) was kept constant, although we estimate theoretically that this factor may increase by perhaps a factor of 2 in the range of absorption covered in this experiment. The broad size distribution of the scatterers was taken into account by averaging our numerical results over particle sizes between 0.2 and 5 μm. The results were found quite independent of the exact choice of the particle size distribution. As shown in Fig. 15, they show good agreement with the experimental results. Note that no adjustable parameters are used, as all of them were determined experimentally. The good agreement suggests that the observed wavelength dependence of the photonic Hall effect η is mainly due to the effect of absorption on the magneto cross section of one Mie particle. Our numerical study can be summarized by the simple relation

$$\eta = (\alpha + \beta\kappa_s)V_s B_0 \ell^* , \tag{25}$$

where α and β are parameters that may depend on sample geometry, refractive index contrast, size- and shape-distribution of the scatterers, etc., but not on the Verdet constant, absorption of the matrix, or magnetic field and concentration.

3.4.4   Photonic Magnetoresistance

Now that the analogy between the electronic and the photonic Hall effect seems to be well established, one can wonder whether electronic magnetoresistance also has a photonic equivalent. The photonic magnetoresistance was measured by performing phase-sensitive detection at 2Ω on the magnetically induced change of the transmitted intensity and normalizing by the total transmitted intensity. In this experiment, the magnetic field was aligned perpendicularly to the direction of transmission (see inset, Fig. 16). This ratio is then taken equal to the ratio of the magnetoresistive and normal diffusion coefficients, as expressed by (23). Based on the outcome (21) for Rayleigh scatterers, we used the relation,

$$\frac{\Delta T}{T} \sim -\left(fVB_0\ell^*\right)^2 , \tag{26}$$

as a starting point for our experiments.

Figure 16 shows our results for the transmission modulation at 2Ω as a function of the square of the magnetic field amplitude. Both curves, measured for different particle sizes and for different volume fractions, reveal a quadratic field dependence. From the lock-in phase, we deduce that for these samples, the transmission decreases with increasing magnetic field, i. e., $\Delta I/I \propto -B^2$.

As in the photonic Hall effect, the explicit dependence of the transmission modulation on the Verdet constant can be conveniently studied by varying the temperature. Figure 17 shows the relative transmission modulation at 2Ω
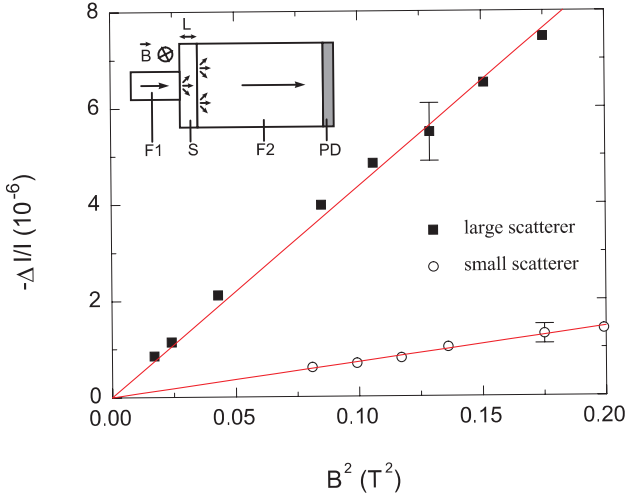
Fig. 16. Transmission modulation at 2Ω versus the square of the magnetic field strength. Temperature is 105 K. Full symbols represent samples with an average particle diameter of 2 µm and a volume fraction $f = 17\%$. Open symbols are for an average particle diameter of 0.4 µm and a volume fraction $f = 10\%$. *Lines are fit to the data points. The inset shows a schematic setup. Light is guided through an optical fiber F1 (diameter 1 mm) to the sample S, which consists of EuF$_2$ powder in a polymer disk. Forwardly scattered light is collected by a light guide F2 and detected by a silicon photodiode PD outside the magnetic field region. The magnetic field is directed perpendicularly to the plane of the drawing. Taken from Sparenberg et al. [43]*

as a function of the square of the inverse temperature at constant magnetic field. The observed linear dependence confirms the quadratic dependence of the photonic magnetoresistance on V.

On the basis of (26), we expect that the magnetoresistance should become independent of f, once we are in the diffusive regime. This is demonstrated in Fig. 18: for high volume fractions, where ℓ^* is smaller than the sample thickness, the observed transmission modulation is independent of f. For low volume fractions, the mean free path is no longer small compared to the sample thickness, and diffusion theory should break down. Experimentally, we see that at low concentrations, the transmission modulation is proportional to the concentration, which is consistent with what may be anticipated from low order scattering events. In the diffusive regime, the data shown in Fig. 18 all fall on the same curve when plotted against the square of ℓ^*. This indicates that that the proportionality factor in (26) is independent of scatterer size.

We conclude that (26) qualitatively covers our observations of photonic magnetoresistance. This identifies the Faraday effect as the underlying mechanism. Now, we come to a quantitative comparison. Using relation (23), we obtain the value $\Delta D_\perp/D_0 \approx -3 \times 10^{-5}\text{T}^{-2}$ for the 0.4 µm particles and
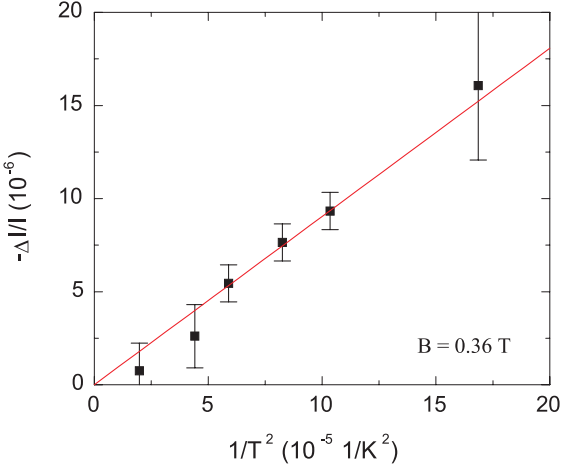
Fig. 17. Transmission modulation (magnetoconductance) at 2Ω versus the inverse square of the temperature. Sample is EuF_2 powder in a polymer disk, subject to a magnetic field of $B = 0.36$ T. The EuF_2 particles have an average diameter of 0.4 μm and volume fraction $f = 17\%$. *Solid line* is a linear fit to the data points. Taken from *Sparenberg* et al. [43]

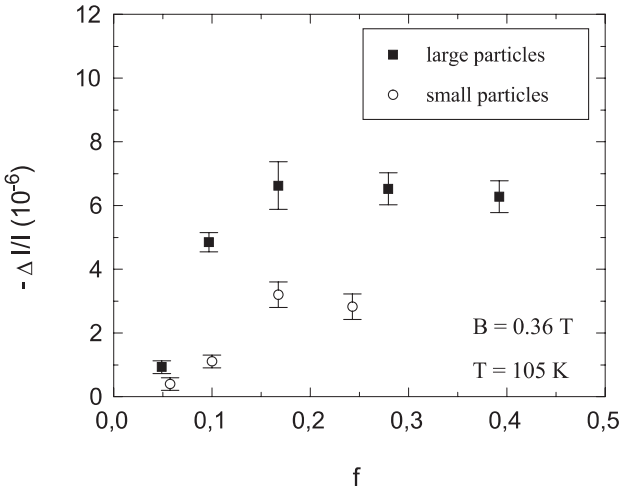**Fig. 18.** Transmission modulation (magnetoconductance) at 2Ω versus the volume fraction of the EuF_2 scatterers, observed at a wavelength $\lambda = 457$ nm. Full symbols represent samples with an average particle diameter of 2 μm, and open symbols denote an average particle diameter of 0.4 μm. Taken from *Sparenberg* et al. [43]

$\Delta D_\perp / D_0 \approx -7 \times 10^{-5} \mathrm{T}^{-2}$ for the 2- μm particles at 105 K. It is important to note that the theory of [37] is valid only for monodisperse Rayleigh scatterers. The small particles, $d \approx 0.4$ μm, are in the Rayleigh–Gans scattering regime [25], since $|n_\mathrm{s} - n_\mathrm{m}| \ll 1$ and $2(m-1)x \approx 0.4$, where $x \equiv n_\mathrm{m} k\, d/2$ is the so-called size parameter and $m \equiv n_\mathrm{s} / n_\mathrm{m}$. The Rayleigh–Gans theory for spheres [25] gives, for $m = 1.051$ and $d = 0.4$ μm, the value $f \cdot \ell^* = 25$ μm. The difference from our measurement $f \cdot \ell^* \approx 8.3$ μm is sufficiently small to be attributed to systematic errors and polydispersity. By the absence of a Rayleigh–Gans theory for magnetodiffusion, we shall compare our experimental results to the prediction for monodisperse Rayleigh scatterers, that follows directly from (21):

$$\frac{\Delta D_\perp}{D_0} = -\frac{243}{5} m^2 \frac{(Vd)^2}{(m^2-1)^4 x^8}. \tag{27}$$

For the observed range of diameters 0.3 μm $< d <$ 0.5 μm, (27) provides a theoretical range $-2 \times 10^{-6} \mathrm{T}^{-2} > \Delta D_\perp / D_0 > -4 \times 10^{-5} \mathrm{T}^{-2}$, which agrees in sign and order of magnitude with the experimental value $\Delta D_\perp / D_0 \approx -3 \times 10^{-5} \mathrm{T}^{-2}$ at 105 K. The 2- μm scatterers are no longer in the Rayleigh–Gans regime, and a prediction on the basis of Rayleigh scattering theory is even less justifiable. Nevertheless, we emphasize that the scaling relation (26) is found to apply to all samples that we investigated, which strongly suggests that the Faraday effect is the universal mechanism of photonic magnetoresistance.

3.4.5   Conclusions and Acknowledgments

This work has attempted to review our theoretical and experimental studies of the magneto-optics of random media. A magnetic field breaks time-reversal symmetry in light propagation; the most well-known manifestation of this breaking is the Faraday effect. Our study therefore contributes to the more general study of waves in complex media [44] with broken spatial or temporal symmetries, like human tissue and seismic media, or highly disordered media. At the same time, since the magnetic field enables us to manipulate the phase shifts of the multiply scattered light waves externally, magneto-optical studies are in many ways the "photonic equivalents" of the successful mesoscopic studies of charge transport in a magnetic field.

Most of this work was carried out in close collaboration with our students Anja Sparenberg, David Lacoste, Georg Düchs, Sabine Wiebel, Anne Napierala, and Cornelius Strohm whom we would like to thank for their efforts and enthusiasm. It is a pleasure to thank Profs. Roger Maynard and Peter Wyder for their continuous interest and support.

Note Added in Proof

Magneto-transverse scattering has recently also been seen for surface-plasmon polaritons (G. Düchs, A. Sparenberg, G. L. J. A. Rikken, P. Wyder, Phys. Rev. Lett. **87**, 127902-1 (2001)

References

1. J. P. Gordon: Phys.Rev. A **8**, 14 (1973) 275
2. I. Brevik: Phys. Rep. **52**, 133 (1979) 275
3. R. Peierls: *More Surprises in Theoretical Physics*, (Princeton University Press, Princeton 1991) 275
4. J. D. Jackson: *Classical Electrodynamics* (Wiley, New York 1975) 275, 279
5. L. D. Landau, E. M. Lifshitz, L. P. Pitaevskii: *Electrodynamics of Continuous Media* (Pergamon, Oxford 1984) 276, 277, 278
6. Ping Sheng: *Introduction in Wave Scattering, Localization and Mesoscopic Physics* (Academic, San Diego 1995) 276, 282, 284, 285
7. Research Group POAN (Ed): *New Aspects of Electromagnetic and Acoustic Wave Diffusion* (Springer, Berlin, Heidelberg, 1998) 276
8. A. Lagendijk, B. A. van Tiggelen: Phys. Rep. **270**, 143 (1996) 276
9. N. B. Baranova, B. Ya. Zel'dovich: JETP Lett. **509**, 681 (1994) 278
10. R. Schlesser, A. Weis: Opt. Lett. **14**, 1015 (1992) 278
11. G. W. 't Hooft, M. B. van der Mark: Nature **381**, 27 (1996) 278
12. D. F. Nelson: Phys. Rev. Lett. **76**, 4713 (1996) 278
13. Y. Jiang, M. Liu: Phys. Rev. Lett. **77**, 1043 (1996) 278
14. M. F. Bishop, A. A. Maradudin: Phys. Rev. B **14**, 3384 (1976) 278
15. A. Puri, J. L. Birman: Phys. Rev. A **27**, 1044 (1983) 278
16. M. Born, E. Wolf: *Principles of Optics* (Pergamon, Oxford 1980) 279
17. R. P. Feynman, R. B. Leighton, M. Sands: *The Feynman Lectures on Physics*, Vol. II, Sect. 27–4 (Addison-Wesley, Reading 1979) 279
18. J. A. Stratton: *Electromagnetic Theory* (McGraw-Hill, New York 1941) Sect. 2–19 279
19. G. L. J. A. Rikken, B. A. van Tiggelen: Phys. Rev. Lett. **78**, 847 (1997) 279, 280
20. G. W.'t Hooft, G. Nienhuis, J. C. J. Paaschens: Phys. Rev. Lett. **80**, 1114 (1998) 280
21. G. L. J. A. Rikken, B. A. van Tiggelen: Phys. Rev. Lett. **80**, 1115 (1998) 280, 290
22. G. L. J. A. Rikken, B. A. van Tiggelen: Nature **381**, 54 (1996) 285, 292, 294
23. I. Campos, J. L. Jiménez: Eur. J. Phys. **13**, 117 (1992) 281
24. G. W. Ford, S. A. Werner: Phys. Rev. B **18**, 6752 (1978) 281
25. H. C. van de Hulst: *Light Scattering by Small Particles* (Dover, New York 1981) 281, 285, 299
26. D. Lacoste, B. A. van Tiggelen, G. L. J. A. Rikken, A. Sparenberg: J. Opt. Soc. Am. A **15**, 1636 (1998) 281, 282, 283, 295
27. F. Erbacher, R. Lenke, G. Maret: Europhys. Lett. **21**, 551 (1993) 284
28. R. Lenke: Diffusion Multiple de la Lumière: Déstruction de la Rétrodiffusion Cohérente par la Rotation Faraday Magnéto-optique. Ph.D. Thesis, Université Joseph Fourier, Grenoble (1994) 284
29. A. S. Martinez, R. Maynard: Phys. Rev. B **50**, 3714 (1994) 284, 290
30. F. C. MacKintosh, S. John: Phys. Rev B **37**, 1884 (1988) 284
31. D. Lacoste, B. A. van Tiggelen: Phys. Rev. E **61**, 4556 (2000) 284
32. J. J. M. Beenakker, G. Scoles, H. F. P. Knaap, R. M. Jonkman: Phys. Lett. **2**, 5 (1962) 284

33. D. Lacoste, B. A. van Tiggelen: Europhys. Lett. **45**, 721 (1999) 285, 286, 289, 295

34. D. Lacoste: Diffusion de la Lumière dans les Milieux Magnéto-optiques ou Chiraux. Ph.D. Thesis, Université Joseph Fourier, Grenoble (1999) 285, 289

35. B. A. van Tiggelen: Phys. Rev. Lett. **75**, 422 (1995) 285, 289

36. N. W. Ashcroft, N. D. Mermin: *Solid State Physics* (Holt, New York 1976) App. E 285

37. B. A. van Tiggelen, R. Maynard and Th.M. Nieuwenhuizen: Phys. Rev. E **53**, 2881 (1996) 285, 299

38. J. H. Li, A. A. Lisyansky, T. D. Cheung, D. Livdan, A. Z. Genack: Europhys. Lett. **22**, 675 (1993) 287

39. G. Düchs, A. Sparenberg, G. L. J. A. Rikken, B. A. van Tiggelen: Phys. Rev. E. **62**, 2840 (2000) 290, 291, 292, 293

40. S. Wiebel, A. Sparenberg, G. L. J. A. Rikken, D. Lacoste, B. A. van Tiggelen: Phys. Rev. E. **62**, 8636 (2000) 293, 294, 295

41. C. Görller-Walrand, H. Peeters, Y. Beyens, N. de Moitié-Neyt, M. Behets: Nouv. J. Chim. **4**, 715 (1980) 294

42. G. L. J. A. Rikken, A. Sparenberg, B. A. van Tiggelen: Physica B **246, 247**, 188 (1998) 288, 289, 294

43. A. Sparenberg, G. L. J. A. Rikken, B. A. van Tiggelen: Phys. Rev. Lett. **79**, 757 (1997) 297, 298

44. J. P. Fouque (Ed.): *Wave Diffusion in Complex Media* (Kluwer, Dordrecht 1999) 299

Index